J Eng Math (2006) 56:307–322
DOI 10.1007/s10665-006-9085-7

ORIGINAL PAPER

A diagonal-mass-matrix triangular-spectral-element method based on cubature points

F. X. Giraldo · M. A. Taylor

Received: 21 December 2005/Accepted: 21 July 2006 /
Published online: 10 November 2006

Abstract The cornerstone of nodal spectral-element methods is the co-location of the interpolation and integration points, yielding a diagonal mass matrix that is efficient for time-integration. On quadrilateral elements, Legendre–Gauss–Lobatto points are both good interpolation and integration points; on triangles, analogous points have not yet been found. In this paper, a promising set of points for the triangle that were only available for polynomial degree $N \leq 5$ are used. However, the derivation of these points is generalized to obtain degree $N \leq 7$ points, which are referred to as *cubature points* because their selection is based on their integration accuracy. The diagonal-mass-matrix (DMM) triangular-spectral-element (TSE) method based on these points can be used for any set of equations and any type of domain. Because these cubature points integrate up to order $2N$ along the element boundaries and yield a diagonal mass matrix, they allow the triangular spectral elements to compete with quadrilateral spectral elements in terms of both accuracy and efficiency, while offering more geometric flexibility in the choice of grids. It is shown how to implement this DMM TSE for a variety of applications involving elliptic and hyperbolic equations on different domains. The DMM TSE method yields comparable accuracy to the exact integration (non-DMM) TSE method, while being far more efficient for time-dependent problems.

Keywords Elliptic · Hyperbolic · Mass · Lumped · Triangle

1 Introduction

Finite-element methods were initially applied to self-adjoint operators (e.g., elliptic equations), but eventually found widespread use in non-self-adjoint operators such as those arising from hyperbolic equations. For many applications, especially those having smooth solutions (i.e., infinitely differentiable), it is far more efficient to use high-order instead of low-order methods. On quadrilateral elements, high-order accuracy is obtained by using the nodal polynomial basis generated from a tensor product of the

F. X. Giraldo (✉)
Naval Postgraduate School, Monterey, CA 93943, USA
e-mail: giraldo@nrlmry.navy.mil

M. A. Taylor
Sandia National Laboratory, Albuquerque, NM 87185, USA

Legendre–Gauss–Lobatto (LGL) points; these points have both good polynomial interpolation and integration (cubature) properties. This approach was introduced by Patera [1] and dubbed the *spectral element* method.

The importance of the LGL set to the diagonal-mass-matrix spectral-element method (DMM SE) cannot be understated. In the square, a $(N+1)\times(N+1)$ tensor product of LGL points has a near-optimal Lebesgue constant for the polynomial space $\mathcal{Q}_N = \text{span}\{\xi^n\eta^m, m, n \le N\}$. This small Lebesgue constant means the LGL points generate a well-conditioned nodal basis for $\mathcal{Q}_N$. By nodal basis, we mean the Lagrange interpolating polynomials associated with the LGL points; these basis functions are also known as cardinal functions. This nodal basis naturally separates into vertex, edge and interior modes, and can be used in a standard $h-p$ finite-element method [2]. In addition, the LGL points interpolating $\mathcal{Q}_N$ have a quadrature formula (cubature in more than one dimension) which will exactly integrate all polynomials in $\mathcal{Q}_{2N-1}$. The inner products that appear in the mass matrix of such a formulation will be polynomials of up to degree $2N$. Thus, a high-quality approximation of these inner products (although not exact) can be obtained by evaluating the integrals using the LGL cubature. Combining this cubature approximation with a nodal basis yields an accurate method with a diagonal mass matrix.

Unfortunately, points analogous to the LGL points do not appear to exist for the triangle. Thus, spectral-element methods in triangles have focused on two different approaches. In the first approach, a more traditional basis of vertex, edge and interior modes is used to construct C_0 test functions, and cubature formulas for the triangle are used to exactly evaluate the resultant inner products (see [3]); this approach results in a *modal* triangular spectral-element method. In the second approach, a nodal basis is constructed using nodal sets in the triangle with a small Lebesgue constant. These points must be found numerically (see [4, 5]). They can then be coupled with exact cubature formulas, resulting in a *nodal space* approximation where two different sets of points are used for interpolation (Fekete points) and integration (Gauss points) [6, 7]); this approach results in a *nodal* triangular spectral-element method. Both the *modal* and *nodal* high-order triangular finite-element approaches yield exponential (or spectral) convergence, and for this reason are known as either *spectral elements* or *spectral/hp elements*. The difficulty that these methods face is that they both require the inversion of a sparse global mass matrix because the interpolation and integration points are not co-located as in the quadrilateral case. Thus, these two triangle-based approaches cannot compete in terms of efficiency with quadrilateral-based spectral elements.

For this reason, attempts have been made to construct triangular-spectral-element (TSE) methods with diagonal mass matrices (DMM) [8, 9, 10]. The reason for developing triangular high-order methods is that the triangle (2-simplex) is much more geometrically flexible than quadrilaterals for constructing grids, especially for complex domains. In the past, to make triangular finite-element methods more efficient, mass lumping had been used which, as pointed out by Cohen et al. [8], is related to seeking co-located interpolation and integration points. However, such points for the triangle are not easy to derive. Cohen et al. [11] obtained points for degree $N=2$ and $N=3$ in the triangle by enriching the polynomial space with additional interior modes that vanish at the edges and vertices of the elements and increase the cubature accuracy. Following similar ideas, Mulder [12] obtained points of degree $N=4$ and $N=5$. Because these points are constructed with integration accuracy in mind, we refer to them as *cubature points*. We will generalize the approach for deriving these cubature points to rederive the sets $N=1,...,5$, and also derive two new sets $N=6$ and $N=7$, keeping in mind that higher-degree sets can be achieved with this approach. The main goal of this paper, however, is to show how to build numerical models for various partial differential equations using these cubature points.

Section 2 describes the discretization of the governing equations. This section includes a description of the construction of the cubature points, Lagrange cardinal functions, and Vandermonde matrix required for the construction of the spatial filter. The construction of a quality filter appears to be the key to the successful implementation of the cubature points. In Sect. 3, we present convergence rates for the DMM TSE method and compare it with the non-DMM TSE developed in [7]. This then leads to certain conclusions about the feasibility of this approach for possible use in various applications.

2 Spatial discretization

In this section, we describe the spatial discretization of the governing equations by the DMM TSE method including: derivation of the cubature points, the choice of basis functions, and the Vandermonde matrix used for filtering. However, before discussing these issues, we first review a few relevant issues concerning interpolation and cubature.

2.1 Interpolation in the reference element

We start by presenting some definitions and introducing our notation in the reference element T. Let $z = (\xi, \eta)$ be a point in $\mathbf{R}^2$, and let T be the right triangle given by

$T = \{(\xi, \eta) \mid -1 \leq \xi, \eta \leq 1; \xi + \eta \leq 0\}$.

Let $\mathcal{P}_N$ denote the traditional space of all polynomials of degree $\leq N$,

$\mathcal{P}_N = \text{span}\{\xi^n \eta^m, m + n \leq N\}$.

Here, following [8] we will be working in an augmented space of polynomials denoted by $\mathcal{P}_{N,M}$. To construct this space, we first let $\mathcal{P}_N^0$ denote the space spanned by the interior modes,

$\mathcal{P}_N^0 = \{f \in \mathcal{P}_N \mid f(z) = 0 \quad \forall z \in \partial T\}$,

where ∂T is the boundary of T. The augmented space $\mathcal{P}_{N,M}$ is then given by adding interior modes to the space $\mathcal{P}_N$,

$\mathcal{P}_{N,M} = \mathcal{P}_N \cup \mathcal{P}_{(N+M)}^0$,

for $M \geq 0$. Thus, $\mathcal{P}_{N,M}$ is the space of polynomials up to at most degree N along the boundary and up to degree $N + M$ in the interior. Note that $\mathcal{P}_N = \mathcal{P}_{N,0}$ and

$\mathcal{P}_N \subset \mathcal{P}_{N,M} \subset \mathcal{P}_{(N+M)}$.

Also, $\dim\mathcal{P}_N = (N + 1)(N + 2)/2$ and, for $N \geq 3$, $\dim\mathcal{P}_{N,M} = \dim\mathcal{P}_N + M(N - 3) + (M + 1)/2$.

Now consider a set of K points in the triangle T, $\{z_i = (\xi_i, \eta_i), i = 1, \ldots, K\}$, with $K = \dim\mathcal{P}_{N,M}$. If the points are non-degenerate, the nodal basis for $\mathcal{P}_{N,M}$ can be defined uniquely as the cardinal functions in $\mathcal{P}_{N,M}$ that satisfy

$$\psi_i(z) = \begin{cases} 1, & \text{if } z = z_{\text{i}} \\ 0, & \text{if } z = z_{\text{j}}\ j \neq i \end{cases}. \tag{1}$$

The nodal basis is directly related to interpolation, since for an arbitrary function q the interpolant $I(q) \in \mathcal{P}_{N,M}$ is given by

$$I(q) = \sum_{i=1}^{K} q(z_i)\psi_i(z),$$

where $I(q)(z_i) = q(z_i)$. The quality of the interpolation operator (and thus of the nodal basis) for a given space and set of points is usually measured by the Lebesgue constant $\|I\|$ (the L^∞-norm of the interpolation operator).

2.2 Cubature in the reference element

Now we turn to the cubature properties of the points z_i. A cubature rule for these points and weights w_i is of strength d, if and only if

$$\int_T g = \sum_{i=1}^{K} w_i g(z_i) \quad \forall g \in \mathcal{P}_d. \tag{2}$$

Any set of $K = \dim\mathcal{P}_{N,M}$ non-degenerate points $\{z_i\}$ will have a cubature rule of at least strength N by using the generalized Newton–Cotes weights,

$$w_i = \int_T \psi_i.$$

Because of Eq. 1, this choice gives a quadrature rule that exactly integrates the cardinal functions, ψ_i. Since these functions are a basis for $\mathcal{P}_{N,M}$, the cubature rule is exact for all $g \in \mathcal{P}_{N,M}$, and thus for all $g \in \mathcal{P}_N$ and so the cubature rule is at least of strength N. However, for some point sets, the Newton–Cotes quadrature formula will integrate a larger space, and the cubature rule can be of strength $2N$ or higher.

As mentioned in the Introduction, for the 1-simplex and its tensor products, the LGL points of degree N are both optimal interpolation and cubature points. Thus, a highly accurate method can be developed resulting in a diagonal mass matrix since the interpolation and integration points are co-located; having a diagonal mass matrix is important for achieving efficiency. On the 2-simplex, such points have not yet been found and one must be content to choose either good interpolation or integration but not both.

It should be noted that in previous works the Fekete points have been used as integration points to obtain a diagonal mass matrix [9, 13]; however, the cubature rule for Fekete points of degree N is only of strength N, and thus using these cubature points is a poor approximation to the degree $2N$ inner products which appear in the integral formulation of the equations. For certain problems, cubature of strength N is insufficient to achieve exponential convergence. An example is shown in Fig. 1 for test 3 given in Sect. 3. The dashed line denotes the solution obtained with Fekete points of degree N for interpolation, and Gauss points for integration of strength $2N$ (to achieve a strength of $2N$, the Gauss points are *oversampled*, meaning there are too many of them to be used to construct a degree N nodal basis). These two sets of points working in tandem give extremely good results, with the error remaining flat for long time-integrations; we shall refer to this approach as the Fekete–Gauss method. In contrast, the dotted line shows that, when the Fekete points are used for both interpolation and integration, the fact that these points are only of strength N means that the error rises rather quickly and is significantly larger. The advantage of the latter strategy, however, is that the interpolation and integration points are co-located; that is, they are one and the same. This vastly simplifies the construction of the numerical algorithms because one need not interpolate onto another set of points in order to evaluate integrals. The fact that the interpolation and integration points are co-located means that the mass matrix is diagonal and therefore trivial to invert; a non-diagonal mass matrix has been a thorn in the side of triangular spectral-element methods, and is the main reason why triangles have not been able to compete with quadrilaterals in terms of efficiency.

From this discussion, it seems logical to assume that, to get around the current dilemma, requires the construction of a new set of points for the triangle that have cubature strength close to $2N$ while having

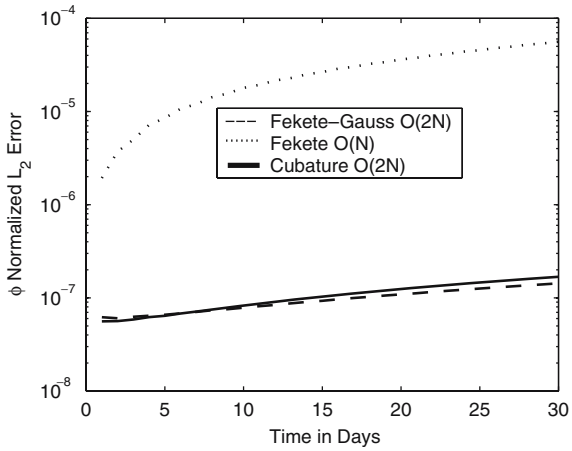

Fig. 1 Test 3: Shallow-water equations. The normalized ϕ L^2 error as a function of time in days for the Fekete–Gauss method with $\mathcal{O}(2N)$ integration (dashed line), Fekete points with $\mathcal{O}(N)$ integration (dotted line), and the cubature points with $\mathcal{O}(2N)$ integration (solid line) integration for $n_I = 3$ and $N = 7$ polynomials

reasonably low Lebesgue constants. In the next section, we describe the approach for constructing points that satisfy both of these two criteria. The solid line in Fig. 1 shows the results for these new cubature points; these points offer a similar accuracy to the Fekete–Gauss set while having the attractive property of the Fekete points, that is, a diagonal mass matrix.

2.3 Computing cubature points

Finding points with optimal cubature properties has been extensively studied independently of spectral-element applications and has a long history of both theoretical and numerical development. For a recent review, see [14–17]. An on-line database containing many of the best known quadrature formulas is described in [18]. One successful approach for numerically finding quadrature formulas dates to [19]. A generalized version was used recently in [20]. Newton's method is used to solve the nonlinear system of algebraic equations for the quadrature weights and locations of the points. Symmetry is used to reduce the complexity of the problem. The complexity can be further reduced with a cardinal-function-based algorithm [21].

If one consults the database and the newest numerical results in the above references, it appears that cubature points of degree N with strength $2N$ or even $2N-1$ do not exist in T. Furthermore, the best cubature formulas for T do not have sufficient points (if any) on the boundary of T. If a set of cubature points will also be used to construct the nodal basis in the space $\mathcal{P}_{N,M}$, there must be $N+1$ points along each edge of T. This is because the nodal basis must generate vertex, edge and interior modes, and the interior modes must be uniformly zero on ∂T (this is critical for the construction of C^0 approximations across element boundaries). If a cardinal function $\psi_i \in \mathcal{P}_{N,M}$ is zero at $N+1$ points on an edge of T, then $\psi_i(z) = 0$ for any point z on that edge. This is because the restriction of any function in $\mathcal{P}_{N,M}$ to that edge is a polynomial of degree N. Thus, any ψ_i for z_i in the interior of T is automatically an interior mode.

Since the goal of achieving a cubature formula using points that interpolate $\mathcal{P}_N$ and are of strength $2N-1$ is not achievable, we follow the ideas first put forth by Cohen et al. [8, 11] and Mulder [12]. Instead of working in $\mathcal{P}_N$, we use the enriched space $\mathcal{P}_{N,M}$ with $M > 0$. A point set that can interpolate $\mathcal{P}_{N,M}$ necessarily contains more points than those for $\mathcal{P}_N$. Thus, there are more degrees of freedom that can be used to satisfy the system of cubature equations given in (2). The resulting points, which we call $\mathcal{P}_{N,M}$ cubature points, are tabulated and compared against the two point sets used in the Fekete–Gauss method in Table 1. The cubature points for $N = 2$ and $N = 3$ are due to Cohen et al. [8, 11] and degrees $N = 4$ and $N = 5$ are due to Mulder [12].

To extend these results, we used the cardinal-function-cubature algorithm of [21]. Straightforward modifications were required, first to work with interpolation points for $\mathcal{P}_{N,M}$ instead of $\mathcal{P}_N$, and second to

Table 1 Properties of the cubature points and the points used in the Fekete–Gauss method

Fekete–Gauss in $\mathcal{P}_N$					Cubature in $\mathcal{P}_N$				
N	K	K'	d	$\|I\|$	N	M	$K = K'$	d	$\|I\|$
1	3	3	2	1.00	1	0	3	1	1.00
2	6	6	4	1.67	2	1	7	3	1.45
3	10	12	6	2.11	3	1	12	5	2.21
4	15	16	8	2.58	4	1	18	7	3.75
5	21	25	10	3.19	5	2	30	10	5.23
6	28	36	12	4.08	6	3	46	12	7.40
7	36	46	14	4.78	7	3	51	14	7.50

N and M determine the polynomial space $\mathcal{P}_{N,M}$, K is the number of interpolation points, K' the number of integration points, d the strength of the integration points and $\|I\|$ is the Lebesgue constant of the interpolation points

impose that there be $N+1$ points along each edge of T (for a total of $3N$ points along the perimeter). We were able to reproduce the previously computed results for degrees $N \leq 5$ along with the two new degrees $N = 6$ and $N = 7$, which we list in Table 2. In fact, higher degrees of N for either triangles or tetrahedra are achievable with this procedure.

Table 1 shows the number of interpolation points, K, integration points, K', and Lebesgue constant, $\|I\|$, for both the Fekete–Gauss and cubature points as a function of the polynomial degree, N. The first thing to notice about these two sets is that the Fekete–Gauss points have superior Lebesgue constants than the cubature points. However, this should not be surprising, since the Fekete points are constructed by minimizing interpolation error, and the Lebesgue constant is a measure of the quality of the points to achieve good interpolation (a lower Lebesgue constant implies better interpolation).

2.4 Evaluating the nodal basis functions

To define the local operators used to construct the global approximation of the solution, we begin by decomposing the domain Ω into N_e non-overlapping triangular elements Ω_e such that

$$\Omega = \bigcup_{\mathrm{e}=1}^{N_\mathrm{e}} \Omega_\mathrm{e}.$$

We then further map the arbitrary triangles Ω_e into the reference right triangle T. To perform differentiation and integration operations, we introduce the nonsingular mapping $\boldsymbol{x} = \Psi(\boldsymbol{\xi})$ that defines a transformation from the physical Cartesian coordinate system, $\boldsymbol{x}$, within each triangle Ω_e to a local reference coordinate system, $\boldsymbol{\xi}$, in the reference right triangle T (see [7] for details on this mapping for curved elements in $\mathbf{R}^3$).

Let us now represent the local element-wise solution q by its nodal expansion in $\mathcal{P}_{N,M}$, as

$$q(\boldsymbol{\xi}) = \sum_{k=1}^{K} q(\boldsymbol{\xi}_k)\psi_k(\boldsymbol{\xi}),$$

Table 2 The polynomial order, N, number of cubature points, and x and y values of the first two barycentric coordinates of the cubature points corresponding to this cubature weight. The third barycentric coordinate is defined such that the all three coordinates add up to one

N	Number	x	y	weight
6	1	0.3333333333333333	0.3333333333333333	0.0340548001889250
	3	0.0000000000000000	0.0000000000000000	0.0004842730760035
	3	0.4207074595153500	0.1585850809708500	0.0177785008242257
	3	0.6975345054486999	0.1512327472752000	0.0122972050038037
	3	0.5000000000000000	0.0000000000000000	0.0032466690489985
	3	0.0484777152220000	0.9030445695557999	0.0080400015624530
	6	0.1009333864342500	0.0000000000000000	0.0020317308565252
	6	0.2688476619807000	0.0000000000000000	0.0030227165121272
	6	0.3694234213017000	0.0497413284926000	0.0171924926133297
	6	0.2841797219605000	0.1685399500274000	0.0202547332903523
	6	0.1811513191269000	0.0548913882427000	0.0142325352719635
7	3	0.0000000000000000	0.0000000000000000	0.0002270804834076
	3	0.1671653533624000	0.6656692932752000	0.0215081779064107
	3	0.4799846082104500	0.0400307835790500	0.0142371781018152
	3	0.2805588962964500	0.4388822074071001	0.0236326025323162
	3	0.9336675298564999	0.0331662350717500	0.0041445630524500
	6	0.0797278918581500	0.0000000000000000	0.0011906918877981
	6	0.2013629039284500	0.0000000000000000	0.0020909447779454
	6	0.3789551577387000	0.0000000000000000	0.0026709648805728
	6	0.3428699782753000	0.1406581918813000	0.0211675487584138
	6	0.2809834462433500	0.0493368139566500	0.0139626184559205
	6	0.1321756636294500	0.0499184036996000	0.0103757635344830

where $K = \dim\mathcal{P}_{N,M}$ and the nodal basis functions ψ_k are defined as in (1). For the points (ξ_i, η_j), we choose the newly derived cubature points which, while allowing for simple evaluation of the nodal basis functions, complicate any other operation such as the evaluation of their derivatives. Here, we follow [9] and represent the nodal basis functions in terms of the Proriol polynomials [22, 23] which in T are an orthogonal basis for $\mathcal{P}_{(N,0)}$. Stable recurrence relations can be used to evaluate these polynomials and their derivatives [24]. Note that these polynomials are traditionally denoted with a double index (m,n) representing the top degree in ξ and η. But here, we use a single index and denote them by φ_i, $i = 1, \ldots, \dim\mathcal{P}_N$. To generate an easily computable basis for $\mathcal{P}_{N,M}$, we need to add additional basis functions for the interior modes in $\mathcal{P}_{N,M}$ that are not in $\mathcal{P}_N$. For these polynomials we use the formulas given in [2, 24], denoted by φ_i, $i = (\dim\mathcal{P}_N + 1), \ldots, K$.

2.5 Filtering the high-frequency waves

As with most high-order methods, when solving nonlinear problems, some filtering is needed to control the accumulation of aliasing errors. The ability to selectively filter only the highest wave numbers is an advantage of the spectral-element method. However, it does require that we use an expansion in only orthogonal Proriol polynomials, since a nodal expansion or an expansion that involves interior modes will not be orthogonal, and thus will not isolate the high-frequency content to only the high-wave-number modes.

Thus, to implement filters, we need to compute the expansion of the local element-wise solution q in terms of only orthogonal Proriol polynomials. In order to prevent confusion with the augmented basis for $\mathcal{P}_{N,M}$, here we denote the basis for $\mathcal{P}_{(N+M)}$ by $g_i, i = 1, \ldots, K_1$, where $K_1 = \dim\mathcal{P}_{(N+M)}$.

Since $q \in \mathcal{P}_{N,M} \subset \mathcal{P}_{(N+M)}$, q has a unique expansion in terms of g. Denoting this expansion by

$$q(\xi_i, \eta_i) = \sum_{k=1}^{K} \tilde{q}_k R_{i,k}, \tag{3}$$

where $\tilde{q}_k$ are the Proriol coefficients of q and R is the rectangular Vandermonde matrix for the basis g, allows us to define the $K \times K_1$ rectangular Vandermonde matrix R by

$$R_{i,k} = g_k(\xi_i, \eta_i).$$

The appropriate right inverse of R for filtering is constructed as follows: given the set of point values $q(\xi_i, \eta_i)$, the expansion in terms of φ (the basis for $\mathcal{P}_{N,M}$) can be computed by applying V^{-1}, the inverse of the Vandermonde matrix. Because this polynomial is in $\mathcal{P}_{(N+M)}$ and thus has a unique expansion in terms of g (the basis for $\mathcal{P}_{(N+M)}$), we have a mapping from the set of point values $q(\xi_i, \eta_i)$ to the expansion coefficients $\tilde{q}$; let us denote this map by R^r. Applying (3) to expansion coefficients computed with R^r must recover the original grid-point values, and thus $RR^r = I$, where I is the identity matrix. In matrix form, we now write (3) as

$$\mathsf{q} = \mathsf{R}\,\tilde{\mathsf{q}} \qquad \tilde{\mathsf{q}} = \mathsf{R}^r\,\mathsf{q}. \tag{4}$$

We can now apply filters to q directly to its Proriol coefficients in $\mathcal{P}_{(N+M)}$. There are many possible filters, but here, based on past experience [7, 25], we choose the Boyd–Vandeven transfer function [26] which we denote by Λ. Applying the filter to the amplitudes and then transforming to nodal (physical) space is achieved in the following matrix-vector multiply operation

$$\mathsf{q}^F = \mathsf{F}\,\mathsf{q},$$

where

$$\mathsf{F} = \mathsf{R}\,\Lambda\,\mathsf{R}^r \tag{5}$$

is the $K \times K$ filter matrix applied every time step at full strength. However, in the original Boyd–Vandeven filter only the highest modes (polynomials of degree $N + M$) are completely annihilated, and this may be too severe for either quadrilateral spectral elements or exact integration triangular spectral elements. Thus, the issue with the new cubature points is how to view the approximation space which these points span. For example, should one take the degree to be the degree of the edge modes N, or the degree of the interior modes, $N + M$? Let us denote the order of the space which the filter acts on as N_F. In Table 3 we show the values used for filtering the cubature points. As an example, for $\mathcal{P}_{7,3}$ the interpolation functions of the cubature points contain some degree 10 ($N + M$) modes. The filter then acts on all the degree 9 and 10 modes. Unfortunately, we currently have no theory to support our filter choices; though the values listed in Table 3 were found experimentally, they appear to work for a variety of applications.

2.6 Integration and local element-wise operators

In order to complete the discussion of the local element-wise operations required to construct discrete spectral-element operators, we must lastly describe the integration procedure required by the weak formulation of all Galerkin methods. For any two functions f and g, the integration $\mathcal{I}$ proceeds as follows

$$\mathcal{I}[f,g] = \int_{\Omega_e} f(x)g(x)\mathrm{d}x = \sum_{i=1}^{K} w_i \mid J(\xi_i) \mid f(\xi_i)g(\xi_i), \tag{6}$$

where w are the cubature weights and J the Jacobians of the transformation from physical space to the local space of the reference element. Note that, for straight-edged triangles, J and all other metric terms are constant; not so for curved elements.

To simplify the description of the numerical algorithm, we define the following local element operators:

$$M_{ij}^e = \int_{\Omega_e} \psi_i(x)\psi_j(x)\mathrm{d}x, \tag{7}$$

$$L_{ij}^e = \int_{\Omega_e} \nabla\psi_i(x) \cdot \nabla\psi_j(x)\mathrm{d}x, \tag{8}$$

$$\boldsymbol{D}_{ij}^e = \int_{\Omega_e} \psi_i(x)\nabla\psi_j(x)\mathrm{d}x, \tag{9}$$

representing the mass, Laplacian, and differentiation matrices, where $i, j = 1, \ldots, K$.

Equation 6 allows us to rewrite (7), (8), and (9) as

$$M_{ij}^e = w_i \mid J(\xi_i) \mid \delta_{ij}, \tag{10}$$

Table 3 The indices N, M for the polynomial space, the number of cubature points K, and the highest mode unaffected by the filter, N_F

Filtering for $\mathcal{P}_{N,M}$			
N	M	K	N_F
1	0	3	2
2	1	7	3
3	1	12	4
4	1	18	5
5	2	30	6
6	3	46	8
7	3	51	8

$$L_{ij}^{e} = \sum_{i=1}^{K} w_i \mid J(\xi_i) \mid \nabla\psi_i(\xi_i) \cdot \nabla\psi_j(\xi_i), \tag{11}$$

$$\boldsymbol{D}_{ij}^{e} = w_i \mid J(\xi_i) \mid \nabla\psi_j(\xi_i), \tag{12}$$

where δ_{ij} is the Kronecker delta. As (10) shows, having the interpolation and integration points, ξ_i, co-located results in the diagonal mass matrix, M^e, which significantly simplifies the construction of the global matrix problem and its solution.

2.7 Formulation of the method

We follow the generalized diagonal-mass-matrix spectral-element formulation outlined in [9]. This method is based directly on the original DMM spectral element method proposed in [27], except that the domain is decomposed into triangular instead of quadrilateral elements and we are working in the space $\mathcal{P}_{N,M}$. The method proceeds as follows: by piecing together appropriate nodal basis functions in neighboring elements, a set of global functions can be constructed that are C_0 and piecewise polynomial. These global functions are used as the test functions in the weak form of the equations of interest, and the unknowns are expanded in terms of these global functions. The resulting integral equations are decomposed as a sum of integrals over each element. Finally, the quadrature rule associated with the points used to construct the cardinal function basis is used to evaluate each integral. Because of the nodal nature of the global functions, this results in much simplification, including a diagonal mass matrix.

The result is a method that can satisfy the equations globally by simply summing the local element matrices, Eqs. 10–12, to form their global representation [27]. This summation procedure is known as the global assembly or direct stiffness summation. Let us represent this direct stiffness summation (DSS) procedure by the summation operator

$$\bigwedge_{\mathrm{e}=1}^{N_\mathrm{e}}$$

with the mapping $(i, e) \longrightarrow (I)$, where $i = 1, \ldots, K$ are the local element grid points, $e = 1, \ldots, N_\mathrm{e}$ are the spectral elements covering the global domain, and $I = 1, \ldots, N_\mathrm{p}$ are the global grid points. Applying the DSS operator to the local element matrices results in the following global matrices:

$$M = \bigwedge_{\mathrm{e}=1}^{N_\mathrm{e}} M^e, \quad L = \bigwedge_{\mathrm{e}=1}^{N_\mathrm{e}} L^e, \quad \boldsymbol{D} = \bigwedge_{\mathrm{e}=1}^{N_\mathrm{e}} \boldsymbol{D}^e,$$

where M, L, and $\boldsymbol{D}$ are matrices of dimension $N_p \times N_p$, and M is diagonal and therefore trivial to invert.

2.7.1 Poisson equation on the plane

For the Poisson equation

$$\nabla^2 q = f, \tag{13}$$

we define its variational statement as: find $q \in H_0^1(\Omega) \forall \psi \in H^1$ such that

$$-Lq = f, \tag{14}$$

where $H_0^1(\Omega)$ is the space of all functions (with zero Dirichlet boundary conditions) with functions and first derivatives belonging to $L^2(\Omega)$—the space of all functions that are square integrable over Ω. The domain used for this test is $x \in [0, 1] \times [0, 1]$.

2.7.2 Advection equation on the sphere

For the advection equation on the sphere

$$\frac{\partial q}{\partial t} + \boldsymbol{u} \cdot \nabla q = 0, \tag{15}$$

we define the variational statement as: find $q \in H^1(\Omega) \forall \psi \in H^1$ such that

$$\frac{\partial q}{\partial t} = -M^{-1} \boldsymbol{u}^T \boldsymbol{D} q. \tag{16}$$

On the sphere, however, no additional boundary conditions are required other than periodicity which is satisfied by the connectivity of the grid.

2.7.3 Shallow-water equations on the sphere

The shallow-water equations on the sphere are

$$\frac{\partial \boldsymbol{q}}{\partial t} = S(\boldsymbol{q}), \tag{17}$$

$$S(\boldsymbol{q}) = -\begin{pmatrix} \nabla \cdot (\phi \boldsymbol{u}) \\ \boldsymbol{u} \cdot \nabla \boldsymbol{u} + f\,(\boldsymbol{x} \times \boldsymbol{u}) + \nabla \phi + \mu \boldsymbol{x} \end{pmatrix}, \tag{18}$$

where $\boldsymbol{q} = (\phi, \boldsymbol{u}^T)^T$, the nabla operator is defined as $\nabla = (\partial_x, \partial_y, \partial_z)^T$, ϕ is the geopotential height ($\phi = gh$, where g is the gravitational constant and h is the vertical height of the fluid), $\boldsymbol{u} = (u, v, w)^T$ is the Cartesian wind velocity vector, $f = 2\omega z/a$ is the Coriolis parameter, and (ω, a) represent the rotation of the Earth and its radius, respectively.

The term $\mu \boldsymbol{x}$, where $\boldsymbol{x} = (x, y, z)^T$ is the position vector of the grid points, is a fictitious force introduced to constrain the fluid particles to remain on the surface of the sphere (see [7] for details). Note that this equation set represents an initial value problem with no boundary conditions; the only condition required is that of periodicity which is imposed by the geometry of the spherical domain.

The variational statement of the problem is: find $(\phi, \boldsymbol{u}^T)^T \in H^1(\Omega) \forall \psi \in H^1$ such that

$$\frac{\partial \phi}{\partial t} = -M^{-1} \boldsymbol{D}^T (\phi \boldsymbol{u}), \tag{19}$$

$$\frac{\partial \boldsymbol{u}}{\partial t} = -M^{-1} \boldsymbol{u}^T \boldsymbol{D} \boldsymbol{u} - f\,(\boldsymbol{x} \times \boldsymbol{u}) - M^{-1} \boldsymbol{D} \phi - \mu \boldsymbol{x}, \tag{20}$$

where for ϕ and $\boldsymbol{u}$ we choose the polynomial space $\mathcal{P}_{N,M}$-$\mathcal{P}_{N,M}$.

3 Numerical experiments

For the numerical experiments, we use the normalized L^2 error norm

$$\|q\|_{L^2} = \sqrt{\frac{\int_\Omega (q_{\text{exact}} - q)^2 \mathrm{d}\Omega}{\int_\Omega q_{\text{exact}}^2 \,\mathrm{d}\Omega}}$$

to judge the accuracy of the TSE methods. In addition, we compute the order of convergence as an average convergence rate computed over all the grid refinements, where at each grid refinement, n_I, the convergence rate is defined as

$$\text{rate} = \frac{\log\left[\text{error}_{n_I+1}/\text{error}_{n_I}\right]}{\log\left[n_I/(n_I+1)\right]}.$$

The grid refinement parameter n_I determines the number of elements as follows: on the plane the number of elements are $N_E = 2n_I^2$ and on the sphere $N_E = 20n_I^2$.

Three equation sets are used to judge the performance of the DMM TSE method: elliptic (linear scalar) and hyperbolic equations (linear scalar and nonlinear vector). The elliptic (test 1) is solved on the plane, while the hyperbolic equations (tests 2 and 3) are solved on the sphere. The reason why the topology of the domain is important is that a domain without curvature (such as the plane) can be tiled completely with straight-edged triangles, while a domain with curvature must be tiled by curved triangles; the metric terms of straight-edged triangles are constant per element, whereas for curved elements the metric terms vary with the position of the interpolation/integration points within the element. Thus, the application of DMM TSE method on a curved manifold represents a very stringent test for judging the performance of this new method.

In the next sections, we compare the results of the DMM TSE method using cubature points with those of the Fekete–Gauss method. The Fekete–Gauss method has been optimized to both interpolate and integrate with high accuracy. Therefore, these points represent the best possible solutions that one can achieve with nodal triangular spectral elements. It is true that, for curved elements, the metric terms are no longer constant and therefore, for exact integration, one would require perhaps up to $\mathcal{O}(3N)$ integration accuracy; however, because the difference between $\mathcal{O}(3N)$ and $\mathcal{O}(2N)$ integration is minimal, we shall refer to the Fekete–Gauss $\mathcal{O}(2N)$ as the best possible solution that one can achieve with nodal triangular spectral elements.

Of special interest is whether or not the cubature points yield exponential (spectral) convergence; in other words, we are particularly interested if the following relation holds

$$\text{error} \propto \mathcal{O}(\Delta x^{N+1}),$$

which states that the error decreases exponentially with grid refinement (Δx) for increasing polynomial order N. Thus for a method to possess spectral accuracy, a convergence rate of order $(N + 1)$ is required for all values of N.

3.1 Test 1: Poisson equation on the plane

The Poisson equation has the exact solution

$$q_{\text{exact}} = x^a(1-x)^b y^c(1-y)^d,$$

when the forcing function, f, is used to satisfy (13). The coefficients a, b, c, and d control the polynomial degree of the solution and for simplicity we take $a = b = c = d = 3$ which results in a twelfth-order polynomial, which is more than sufficient to judge the accuracy of up to seventh-order cubature points. Homogeneous Dirichlet boundary conditions are used, and the Laplacian operator is inverted using the conjugate-gradient method with point Jacobi iteration.

3.2 Test 2: Advection equation on the sphere

The initial condition used for the advection equation is

$$q(\lambda, \theta, 0) = \mathrm{e}^{-r^2/r_i^2},$$

where

$$r = a\cos^{-1}\left(\sin\theta_i \sin\lambda + \cos\lambda_i \cos\theta \cos(\lambda - \lambda_i)\right), \quad r_i = \frac{a}{3},$$

a is the radius of the sphere, and (λ_i, θ_i) is the initial position of the wave in spherical coordinates; the exact solution can be found in [28]. The time-integration is handled by the explicit second-order backward-difference formula proposed in [29].

While this test case also involves a linear scalar equation, as in test 1, the difference is that this equation is now hyperbolic with the additional degree of difficulty imposed by the curved topology of the spherical domain; curvature in the domain has major consequences because the metric terms (e.g., Jacobians) are no longer constant.

3.3 Test 3: Shallow-water equations on the sphere

To further test the accuracy of the DMM TSE method, we use a system of nonlinear hyperbolic equations, that is, the shallow-water equations on a rotating sphere. Similarly to test 2, this test also poses the additional difficulty of using curved elements to allow the elements to tile the surface of the sphere.

The initial conditions used are those of case 2 in the Williamson et al. [28] shallow-water test suite. Once again, the time-integration is handled by the explicit second-order backward-difference formula.

3.4 Summary of results

Figures 2–4 show the normalized L^2 error as a function of grid resolution, n_I, for various polynomial degrees for the Fekete–Gauss and cubature points for tests 1, 2, and 3, respectively.

For test 1 (elliptic equation on the plane), the cubature points perform better than the Fekete–Gauss method for some degrees of N but do not do as well for others, especially for $N \geq 6$. In fact, for this

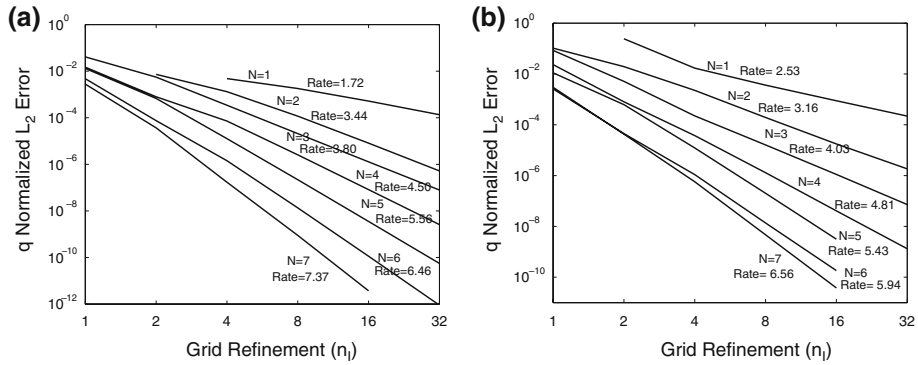

Fig. 2 Test 1: Poisson equation. The normalized q L^2 error for the (**a**) Fekete–Gauss and (**b**) cubature points TSE methods as a function of grid refinement, n_I, for the polynomial degrees $N = 1, \ldots, 7$ with their associated convergence rates

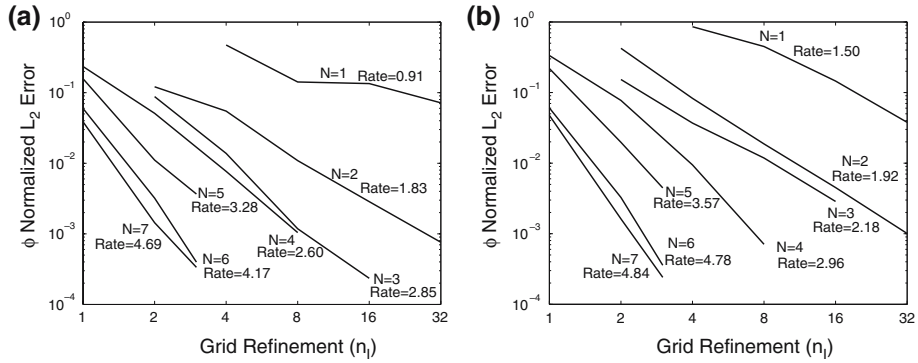

Fig. 3 Test 2: Advection equation. The normalized ϕL^2 error for the (**a**) Fekete–Gauss and (**b**) cubature points TSE methods as a function of grid refinement, n_I, for the polynomial degrees $N = 1, \ldots, 7$ with their associated convergence rates

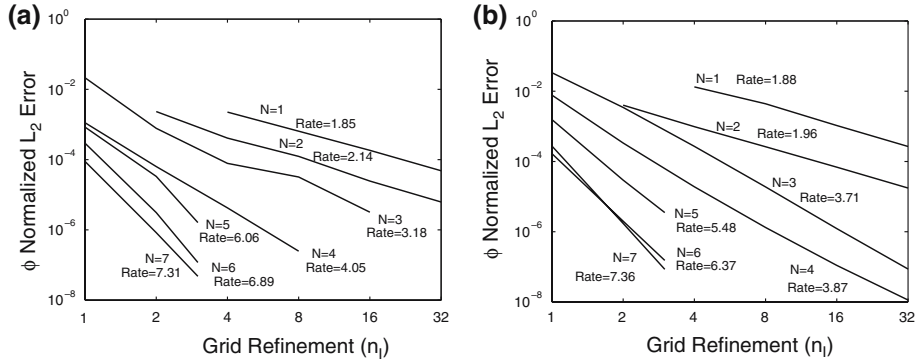

Fig. 4 Test 3: Shallow-water equations. The normalized ϕ L^2 error for the (**a**) Fekete–Gauss and (**b**) cubature points TSE methods as a function of grid refinement, n_I, for the polynomial degrees $N = 1, \ldots, 7$ with their associated convergence rates

particular type of equation, it makes little sense to use the cubature points over the Fekete–Gauss points because both methods require the inversion of a Laplacian and for this reason the cubature points have no advantage; note that the discrete weak-form Laplacian operator is in fact the well-known stiffness matrix.

For test 2 (advection equation on the sphere), both methods failed to yield spectral convergence, even though both methods converged at a rapid rate. However, both methods yield similar convergence rates which is a good result, because it means that the cubature points behave similarly to the Fekete–Gauss points; recall that the Fekete–Gauss points represent the best we can do with high-order nodal triangles.

For test 3 (shallow-water equations on the sphere), the results of the cubature points are similar to those of the Fekete–Gauss method (they both yield spectral convergence); this seems to indicate that the cubature points are a good replacement of the Fekete–Gauss points for systems of nonlinear hyperbolic equations.

From these results, one can see that overall the cubature points do quite well compared to the Fekete–Gauss points. The main reason for considering the cubature points is that they yield a diagonal mass matrix, which allows for the construction of efficient time-integration algorithms. To emphasize this point, we show in Fig. 5 the L^2 error (Fig. 5a) and wall-clock time in seconds (Fig. 5b) as a function of polynomial order for test 3 for both the Fekete–Gauss and cubature-point methods using grid refinement level $n_I = 3$; these results were obtained on a Dell PC with an Intel Xeon 1.8 gigahertz processor. Figure 5a shows that both methods yield spectral convergence, and the errors are almost identical for both methods; however, Fig. 5b shows that the Fekete-Gauss points require far more computing time to achieve these results. The cost of the Fekete–Gauss method increases exponentially with either increasing grid resolution,

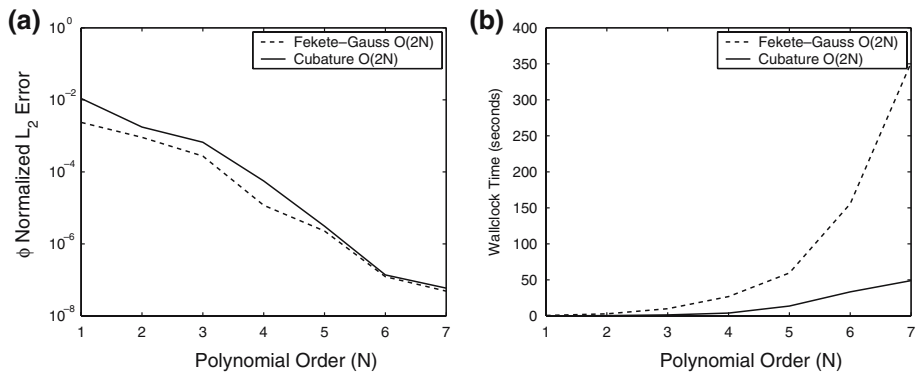

Fig. 5 The (**a**) normalized ϕ L^2 error and (**b**) wallclock time as a function of polynomial order, N, for the Fekete–Gauss and cubature points TSE methods for a five day integration of test 3 using $n_I = 3$ grid refinement

n_I, or polynomial degree, N. This is due to the Fekete–Gauss method having a sparse global mass matrix, which must be inverted at every time step. Giraldo and Warburton [7] showed how to construct this type of nodal triangular spectral element and even with the use of static condensation and conjugate-gradient iterative solvers the cost of the method could not be brought down. In contrast, the cubature points TSE method, having a diagonal mass matrix, allows for very simple and extremely efficient time-integration strategies, precisely because it does not involve the inversion of a mass matrix. In this paper, we have only discussed the repercussions of a diagonal mass matrix on the efficiency of explicit time-integrators; however, these effects are most important in the construction of semi-implicit time-integrators which are used to increase the allowable time-step that a model can use while maintaining stability. Semi-implicit time-integrators play an important role in production-type models such as those used in numerical weather prediction; see [30].

Finally, in Fig. 6 we show the accuracy per computational cost for both the Fekete–Gauss (Fig. 6a) and cubature points (Fig. 6b) for test 3 and orders $N = 1, ..., 7$. The best results are those nearest the bottom left corner of the plots; that is, this means that the method yields high accuracy (low L^2 error) with little computational cost. For the Fekete–Gauss points, the polynomial orders $N = 4$ and $N = 6$ offer the best compromise between accuracy and efficiency. Although the results for these points are not very easy to interpret, one thing is clear: orders $N \leq 3$ are inferior to orders $N \geq 4$. On the other hand, the results of the cubature points are much simpler to interpret. Note that orders $N \leq 2$ are not very competitive with the high order points ($N \geq 3$). Orders $N = 3$ and $N = 4$ give good results, but clearly orders $N \geq 5$ are by far the best. From these three orders, as in the Fekete–Gauss points, order $N = 6$ offers the best compromise between accuracy and efficiency. In summary, the main point of this figure is that high order (in this case $N = 6$) is clearly far more efficient than the lower-order methods. For example, to get an accuracy of 1×10^{-6}, the order $N = 6$ points will cost far less than the other polynomial orders.

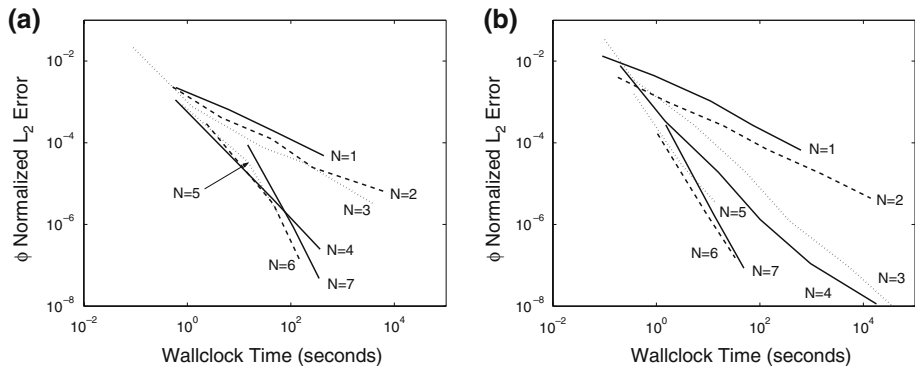

Fig. 6 The normalized ϕ L^2 error as a function of wallclock time for (**a**) the Fekete–Gauss and (**b**) cubature points for a five day integration of test 3 using $N = 1, \ldots, 7$

4 Conclusions

We have presented a promising new set of cubature points on the triangle which can be used both for interpolation and integration. Because the interpolation and integration are co-located, we obtain a diagonal mass matrix (DMM). We have presented implementation strategies of this DMM triangular spectral-element (TSE) method for elliptic and hyperbolic equations on planar and spherical surfaces and compared the cubature points to the usual strategy of employing one set of points for interpolation (Fekete) and another set for integration (Gauss) which we call Fekete–Gauss TSE; this method, however, does not yield a diagonal mass matrix. The cubature points compare quite favorably with the Fekete–Gauss points, especially for the system of nonlinear hyperbolic equations. In addition, these good solutions can

be obtained quite cheaply with the cubature method because they yield a diagonal mass matrix which allows for simple and efficient time-integration strategies; this may now allow the triangular SE method to compete in terms of both accuracy and efficiency with the quadrilateral SE method, while allowing far more flexibility in the choice of adaptive unstructured grids. Because the cubature points yield a DMM TSE, in future work we shall exploit this property to construct semi-implicit time-integrators for various hyperbolic equation sets on adaptive unstructured grids including the Euler equations, and the primitive equations for both the atmosphere and ocean.

Acknowledgements FXG was supported by the Office of Naval Research through program element PE-0602435N. MAT was supported through the Sandia University Research Program. We would like to thank Tim Warburton for his assistance during the initial phase of this work.

References

1. Patera AT (1984) A spectral element method for fluid dynamics — laminar flow in a channel expansion. J Comp Phys 54:468–488
2. Solin P, Segeth K, Dolezel I (2003) Higher-order finite element methods. Chapman and Hall/CRC Press
3. Sherwin SJ, Karniadakis GE (1995) A triangular spectral element method; applications to the incompressible Navier-Stokes equations. Comp Meth Appl Mech Eng 123:189–229
4. Hesthaven JS (1998) From electrostatics to almost optimal nodal sets for polynomial interpolation in a simplex. SIAM J Num Anal 35:655–676
5. Taylor MA, Wingate BA, Vincent RE (2000) An algorithm for computing Fekete points in the triangle. SIAM J Num Anal 38:1707–1720
6. Warburton T, Pavarino LF, Hesthaven JS (2000) A pseudo-spectral scheme for the incompressible Navier–Stokes equations using unstructured nodal elements. J Comp Phys 164:1–21
7. Giraldo FX, Warburton T (2005) A nodal triangle-based spectral element method for the shallow water equations on the sphere. J Comp Phys 207:129–150
8. Cohen G, Joly P, Roberts JE, Tordjman N (2001) Higher order triangular finite elements with mass lumping for the wave equation. SIAM J Num Anal 38:2047–2078
9. Taylor MA, Wingate BA (2000) A generalized diagonal mass matrix spectral element method for non-quadrilateral elements. Appl Num Math 33:259–265
10. Helenbrook B (2004) Polynomial bases suitable for mass lumping on triangles. Int Conf Spectral and High-Order Methods (ICOSAHOM).
11. Cohen G, Joly P, Tordjman N (1995) Higher order triangular finite elements with mass lumping for the wave equation. In: Cohen G, Becahe E, Joly P, Roberts JE (eds) Proc. 3rd Int. Conf. on Mathematical and Numerical Aspects of Wave Propagation. (SIAM, Philadelphia).
12. Mulder WA (2001) Higher-order mass-lumped finite elements for the wave equation. J Comp Acoust 9:671–680
13. Komatitsch D, Martin R, Tromp J, Taylor MA, Wingate BA (2001) Wave propagation in 2-D elastic media using a spectral element method with triangles and quadrangles. J. Comp. Acoustics 9:703–718
14. Cools R, Rabinowitz P (1993) Monomial cubature rules since *Stroud*: a compilation. J Comp and Appl Math 48:309–326
15. Lyness J, Cools R (1994) A survey of numerical cubature over triangles. Appl Math 48:127–150
16. Cools R (1997) Constructing cubature formulae: the science behind the art. Acta Numerica 6:1–54
17. Cools R (1999) Monomial cubature rules since *Stroud*: a compilation — part 2. J Comp Appl Math 112:21–27
18. Cools R (2003) An encyclopaedia of cubature formulas. J Complexity 19:445–453. Online database located at http://www.cs.kuleuven.ac.be/nines/research/ecf/ecf.html
19. Lyness J, Jespersen D (1975) Moderate degree symmetric quadrature rules for the triangle. J Inst Math Appl 15:19–32
20. Wandzura S, Xiao H (2003) Symmetric quadrature rules on a triangle. Comp Math Appl 45:1829–1840
21. Taylor MA, Wingate BA, Bos LP (2006) A cardinal function algorithm for computing multivariate quadrature points. SIAM J Num Anal (to appear)
22. Proriol J (1957) Sur une famille de polynomes á deux variables orthogonaux dans un triangle. C R Acad Sci Paris 257:2459
23. Dubiner M (1991) Spectral methods on triangles and other domains. J Scientific Comp 6:345–390
24. Karniadakis GE, Sherwin SJ (1999) Spectral/hp element methods for CFD, Oxford Univ Press
25. Taylor M, Tribbia J, Iskandarani M (1997) The spectral element method for the shallow water equations on the sphere. J Comp Phys 130:92–108
26. Boyd J (1996) The erfc-log filter and the asymptotics of the Euler and Vandeven sequence accelerations. In: Ilin AV, Scottv LR (eds) Proceedings of the Third International Conference on Spectral and High Order Methods, Houston Journal of Mathematics, Houston, Texas, 267–276

27. Maday Y, Patera AT (1987) Spectral element methods for the incompressible Navier Stokes equations. In: Noor AK, Oden JT, (Eds) state of the art surveys on computational mechanics, ASME, New York, 71–143
28. Williamson DL, Drake JB, Hack JJ, Jakob R, Swarztrauber PN (1992) A standard test set for numerical approximations to the shallow water equations in spherical geometry. J Comp Phys 102:211–224
29. Karniadakis GE, Israeli M, Orszag SA (1991) High-order splitting methods for the incompressible Navier-Stokes equations. J Comp Phys 97:414–443
30. Giraldo FX (2005) Semi-implicit time-integrators for a scalable spectral element atmospheric model. Quart J Roy Meteorol Soci 131:2431–2454